Unravelling the mechanism of amitriptyline removal from water by natural montmorillonite through batch adsorption, molecular simulation and adsorbent characterization studies

Unravelling the mechanism of amitriptyline removal from water by natural montmorillonite through batch adsorption, molecular simulation and adsorbent characterization studies

Po-Hsiang Chang[a], Pan Liu[a], Binoy Sarkar[b,*], Raj Mukhopadhyay[c], Qing-Yuan Yang[d,*], Yu-Min Tzou[e], Bo Zhong[a], Xuxiang Li[a], Gary Owens[f]

[a] School of Human Settlements and Civil Engineering, Xi'an Jiaotong University, 28 Xianning West Road, Xi'an, Shaanxi, 710049, P.R. China

[b] Lancaster Environment Centre, Lancaster University, Lancaster, L A1 4YQ, United Kingdom

[c] Division of Irrigation and Drainage Engineering, ICAR-Central Soil Salinity Research Institute, Karnal 132001, Haryana, India

[d] School of Chemical Engineering and Technology, Xi'an Jiaotong University, 28 Xianning West Road, Xi'an, Shaanxi, 710049, P.R. China

[e] Department of Soil and Environmental Sciences, National Chung Hsing University, 145 Xingda Rd., Taichung, 40227, Taiwan

[f] Environmental Contaminants Group, Future Industries Institute, University of South Australia, Mawson Lakes, SA 5095, Australia

*Co-corresponding authors:

Dr Binoy Sarkar; Lancaster University; email: b.sarkar@lancaster.ac.uk

Prof Qing-Yuan Yang; Xi'an Jiaotong University; email: qingyuan.yang@xjtu.edu.cn

Graphical abstract

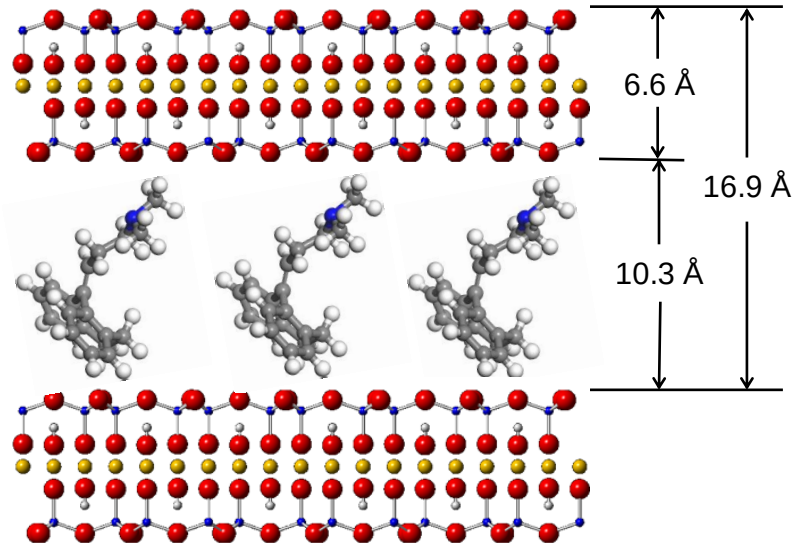

Highlights

- Natural Na-montmorillonite (SWy-2) adsorbed 0.88 meq/g amitriptyline (AMI) from water.
- AMI adsorption was fast (<4 h) and exceeded the clays CEC.
- AMI removal was mainly via a cation exchange mechanism

- AMI removal was unaffected by pH in the range 2 to 11.
- Amine groups and benzene rings in AMI controlled molecular orientation in the clay interlayer.

Abstract

Amitriptyline (AMI) is one of the most common tricyclic antidepressant personal care medications. Due to its environmental persistence and bioaccumulation, release of AMI into the environment via wastewater streams in elevated levels could lead to significant ecological and human health impacts. In this study, the adsorption of AMI by montmorillonite (SWy-2), a naturally abundant smectite clay with sodium ions as the main interlayer cations, was investigated. Maximum AMI adsorption (276 mg/g) occurred at pH 7-8. After adsorption, examination of the adsorbent's X-ray diffraction pattern indicated that interlayer expansion had occurred, where chemical stoichiometry confirmed cation exchange as the principal adsorption mechanism. AMI adsorption reached equilibrium within 4 h, with kinetic data best fitting the pseudo-second order kinetic model ($R^2 = 0.98$). AMI adsorption was unaffected by solution pH in the range 2 to 11, where adsorption was endothermic, and molecular simulations substantiated by Fourier transform infrared spectroscopy and thermogravimetric investigations indicated that the orientation of AMI molecules in the interlayer was via an amine group and a benzene ring.

Overall this research shows that SWy-2 has significant potential as a low cost, effective, and geologically derived natural material for AMI removal in wastewater systems.

Keywords: Adsorption; Amitriptyline; Cation exchange; Molecular simulation; Montmorillonite.

1. Introduction

Organic and inorganic pollutants can both have significant negative impacts on water and soil environments, as well as living organisms, including humans, due to their innate toxicity. The efflux of medical drugs into the environment can thus detrimentally effect ecosystem health and the organisms therein, and is consequently of increasing emerging concern due to the potential for the development of drug induced bacterial resistance as well as damage to ecosystem balance, and plant growth and development [1]. This has resulted from the overuse of many medicinal drugs and the dramatic increase in personal maintenance products. In addition, such pollutants can enter the human body through food chain contamination and cause allergic reactions as well as food poisoning in severe cases [2, 3]. Indeed, many drugs are also known to have carcinogenic, teratogenic, mutagenic or hormonal effects, which seriously interfere with human physiological functions and threaten human health. Thus, there urgently needs to be a range of methods which both reduce the efflux of medicinal drugs into the environment and

where this is unavailable, efficiently remove them from the environment once efflux has occurred.

Clay minerals are naturally available and play an important role in the hydrosphere where they can influence the migration and interaction between organic and inorganic chemicals. Hence, clays have become an important, relatively inexpensive, natural remediating agent for use in the cleanup of environmental contamination [4, 5]. However, the specific mechanisms of interaction between clay minerals and drugs is not clear and needs to be better understood if clays are to be practically used to efficiently remove emerging medicinal drugs from contaminated environments.

Today, there is also an increasing concern that the active compounds present in medical drug formulations constitute a significant pollutant in the aqueous environment, and can thus lead to significant physiological human and animal effects even at very low concentrations. Many medicinal drugs also survive passage through conventional wastewater treatment plants, having been detected in the outlets of sewage treatment plants [6-9], and are thereafter detected in both soil and aqueous systems [10-12]. Furthermore, drugs often produce ecotoxicity, resistance to pathogens, and act as endocrine disruptors to many environmental organisms [8, 13, 14]. Drugs also persist in the environment for a long time, and can therefore be passed to human populations through both food chain contamination and via drinking water. Since many drugs are polar

102 molecules (so that they can be efficiently consumed and absorbed in animal and human systems),
103 which are highly soluble in water, their detection and removal in complex environment matrices
104 is a major challenge [15, 16].
105 Amitriptyline (AMI) is one of the most common tricyclic antidepressant personal care
106 medications, which produces antidepressant effects by inhibiting the reuptake of serotonin and
107 norepinephrine, and is commonly prescribed for the treatment of major depression [17].
108 However, its use is not without some concern, because it is highly toxic with no specific antidote,
109 and can only be used in a narrow safety range to avoid severe poisoning exhibited by strong
110 heart, central system, and respiratory toxicity [18, 19]. Epidemiological studies showed that in
111 the 1990s, tricyclic antidepressant use in Australia and the UK accounted for 8- 12% of all drug
112 overdoses, with a 15- 33% lethality [20, 21]. Thus, after narcotic drugs, tricyclic antidepressants
113 have emerged as the most common harmful drug [18]. While the amount of personal care
114 products discharged into the environment is relatively low compared to the most widely used
115 chemicals, such as pesticides and fertilizers, it would not initially pose a great threat to the
116 environment at low doses, but due to its persistence and accumulation over a long period of time,
117 would lead to significant potential impacts. This indicates that in the future, to prevent the
118 destruction of environmental ecology or reduce the threat to human health, effective means to
119 remove residual medicinal drugs from the environment will be an urgent issue.

Currently, one of the most important research gaps limiting the wider application of clay minerals for the remediation of emerging contaminant drugs is a thorough understanding of the mechanisms of interactions between clay minerals and drugs in contaminated waters. While a wide variety of different pollutants have successfully been removed using a wide variety of different clay modification and removal methods, this study uses a naturally available sodium-rich montmorillonite (Na-montmorillonite) to specifically remove (through adsorption) AMI, which has not been previously reported. As a natural adsorbent, the use of montmorillonite is practically important because it is inexpensive, widely available, and has high cation exchange capacity (CEC), which makes it an outstanding candidate for both industrial and domestic wastewater treatment. Additionally, water treatment with a natural material like montmorillonite also involves minimal greenhouse gas emission, no thermal energy requirement, and minimal risk of secondary pollution. Therefore, in this study the adsorption behavior of the antidepressant drug AMI on SWy-2 was studied as a potential practical remediation technique, and the removal mechanism elucidated by a combination of systematic experiments and molecular simulations.

2. Materials and methods

2.1 Materials

137 The HCl form of AMI (molar mass = 313.87 g/mol; pK_a = 9.4; CAS number 549-18-8) was
138 obtained from Wako Pure Chemical Industries, Ltd., Osaka, Japan [22] (Fig. S1) and had a purity
139 ≥ 98%. The computed molecular size of AMI was 10.68 Å×8.57 Å×5.89 Å [23]. A dioctahedral
140 raw smectite clay, Na-montmorillonite (SWy-2), was obtained from the Clay Minerals Society
141 and used as received. The physicochemical properties of the clay mineral are given in the
142 Supplementary Materials (Table S1). Analytical grade chemicals such as NaOH and HCl were
143 used to adjust the solution pH during the pH effect experiments. An ion chromatographic
144 standard of Na^+, K^+, Mg^{2+} and Ca^{2+} (Custom Mix, 4 Elements, 125 mL mg/L in 5% HNO_3;
145 product number: OTS-160786-02-01) was purchased from www.bgw.org.cn and was used for
146 cation analysis.
147
148 *2.2 Adsorption kinetics, isotherm and regeneration*
149 For the adsorption kinetics study, SWy-2 clay mineral (0.1 g) was mixed with AMI solution (20
150 mL) to give a solid: solution ratio of 1:200 (w/v) and an initial AMI concentration of 500 mg/L
151 in a 50 mL centrifuge tube, and wrapped with aluminum foil to prevent AMI photodegradation.
152 The final solution pH was between 7 to 8, due to the innate buffering action of the clay mineral.
153 The clay mineral-AMI solutions were shaken for 0.25, 0.5, 1.0, 2.0, 4.0, 8.0, 16.0 and 24.0 h.
154 The solid: solution ratio and basic operating conditions in all subsequent experiments were

identical to the kinetic experiments with a few parameter changes based on the goal of that experiment as noted hereafter. For the pH adsorption edge experiment, the equilibrium solution pH was varied between 2 and 11 (where pH was maintained by dropwise judicious addition of either 2*M* NaOH or 2*M* HCl) with an initial AMI concentration of 500 mg/L. For the temperature-dependent adsorption study, temperature was varied and maintained at either 303, 318, or 333 K. During the adsorption isotherm study, the initial AMI concentrations were 50, 100, 200, 300, 400, 500, 600, 700, and 800 mg/L. Choosing such high concentration range of AMI was necessary to properly elucidate the mechanisms of adsorption via physicochemical characterization of the adsorbent so that detectable changes are obtained in the AMI-loaded adsorbent samples. Otherwise, in all experiments, all solutions were shaken on a thermostatic oscillator (SHZ-82) at a constant temperature of 303 K with agitation at 150 rpm for 24 h to ensure equilibrium conditions. After reaching equilibrium, the solutions were then centrifuged (5000 rpm for 5 min), filtered (< 0.22 μm), and analyzed using either an UV-Vis spectrometer or ion chromatography. All experimental studies were conducted in duplicate.

To evaluate thermal regeneration of SWy-2, the adsorbent was initially completely loaded with AMI by reacting the clay mineral (4 g) with a 800 mg/L AMI solution (1600 mL) for 24 h. Preliminary experiments had confirmed that under these conditions, the entire quantity of adsorbent had reached maximum adsorption capacity. Following total AMI adsorption, the

adsorbent clay was separated (by centrifugation at 10,000*g* 20 min) and washed twice with deionized water. The sample was then heated at 600°C in a muffle furnace for 2 h to remove the AMI via thermal decomposition. Finally, the regenerated clay was then reused to conduct the adsorption isotherm experiment again.

The AMI adsorption kinetics data were fitted to pseudo-first order, pseudo-second order, intra-particle diffusion, and Elovich models, while the adsorption isotherm data were fitted to Freundlich and Langmuir models using non-linear fitting methods (Supplementary Materials). For the model fitting exercise, various statistical parameters were calculated, and the values so obtained were compared amongst the various models to determine the optimal model fitting [24] (Supplementary Materials).

2.3 Analysis

AMI concentrations were quantified at 240 nm [25] using a DR5000 UV-Vis spectrometer (Hach, Loveland, USA), where standard AMI solutions were maintained at a similar pH to the samples. Calibration curves were constructed from five standards varying in concentration between 1 and 20 mg/L, and were accepted when $R^2 > 0.999$.

During the adsorption of AMI, cations Na^+, K^+, Mg^{2+}, and Ca^{2+} released (exchanged from the clay mineral) in the solution were analyzed by Integration high-pressure ion chromatography

(HPIC) (Dionex, Thermo Fisher Scientific™, Waltham, USA). Chromatographic retention times for Na^+, K^+, Mg^{2+}, and Ca^{2+} were 2.7, 3.78, 5.92, and 7.38 min, respectively. The instrument was equipped with a Dionex IonPac^{TM} CS12A-5µm column (3×150 mm), and using an aqueous mobile phase of 20 *mM* methanesulfonic acid (1.922 mL in 1L of water) with flow rate of 0.5 mL/min.

X-ray diffraction (XRD) patterns of powdered samples were obtained on a Bruker D8 Advance A25 Diffractometer (Bruker, Hamburg, Germany) with the LynexEye Linear detector and a monochromatic Cu Kα1 (λ=1.54 Å) source. The diffraction patterns were recorded in the 2Θ range of 2-10° with a counting time of 1.25 s/step.

Field emission scanning electron microscope (FE-SEM) images were recorded on a TESCAN MAIA3 Triglav (Ametek, Berwyn, USA) (acceleration voltage:15 kV). The energy dispersion spectrum (EDS) of platinum-coated samples was obtained using an Aztec X-max N50mm^2 detector attached to the SEM.

Thermogravimetric (TG) analyses were conducted under N_2 atmosphere on a NETZSCH STA 449 F5 Jupiter instrument (Netzsch, Deutschland, Germany) (sample weight: 5-10 mg) with a heating rate of 10 °C/min.

Fourier transform infrared (FTIR) analysis of dry powdered samples was carried using the KBr pellet method on a Nicolet iS10 spectrometer (Thermo Fisher Scientific™, Waltham, USA)

(typically 256 scans, resolution 4 cm^{-1}), with scanning in the 4000 to 400 cm^{-1} region.

2.4 Molecular simulation

Molecular simulations were performed to identify AMI intercalation in the interlayer of SWy-2 using the Forcite module of the Materials Studio 2017 software. The model supercell was established by 12 unit cells at 4a×2b×1c. The crystal structure of montmorillonite was characterized by a combination of two-layers of Si-O tetrahedrons (T-layer) with one layer of Al-O octahedrons (O-layer) in between. The TOT layer of montmorillonite (thickness = 6.6 Å) [26] was composed of two oxygen atomic layers and hydrated cations in the interlayer space. Assuming that isomorphic substitution has taken place for Al^{3+} with Mg^{2+} in the octahedral sheet of SWy-2 [$Na_{0.625}Si_8(Al_{3.375}Mg_{0.625})O_{20}(OH)_4$], the total layer charge becomes –5 which is balanced by Na^+ in the interlayer space [27, 28]. Geometric optimization was performed at 303 K with a simulation time of 1 ns and a time step of 1 fs. The computed molecular size of AMI was 10.68 Å×8.57 Å×5.89 Å [23]. The simulation was undertaken in the interlayer space of the clay mineral during AMI adsorption by cation exchange by allowing specific interaction of positively charged AMI functional groups with the crystal layers.

3. Results and discussion

3.1 Kinetics of adsorption

Studies of adsorption kinetics of AMI on Na-montmorillonite showed that equilibrium was reached in about 4 h (Fig. 1). Previous reports suggested that the adsorption of AMI on to Ca-montmorillonite and palygorskite reached equilibrium much more quickly, in about 1 h and within a few minutes, respectively [15, 16]. Among the four kinetic models evaluated, namely pseudo-first order, pseudo-second order, intra-particle diffusion, and Elovich model (Supplementary Material; Fig. S2), the adsorption data were best fitted to the pseudo-second-order kinetic model (R^2 = 0.98; ratio of performance to the deviation (RPD) = 6.97) (Table 1). As calculated from the pseudo-second order model fit [29], the equilibrium constant for AMI adsorption on SWy-2 was 0.02 g/mg.h, and the corresponding equilibrium amount adsorbed (q_e) was 201 mg/g (Table 1). Thus, the q_e value obtained from kinetic data agreed reasonably with the calculated value of 276 mg/g obtained from the well-established Langmuir adsorption isotherm of AMI (Table 2) [30]. The adsorption kinetic data suggested that over time AMI adsorption became a rate-limiting step [30-34]. Compliance with the pseudo-second order model alone cannot by itself be used to infer either a surface-controlled adsorption process or chemisorption as is often assumed [34]. Thus, the validity of the pseudo-second order model for this system was further substantiated by considering other boundary parameters such as the equilibrium or rate constant, the initial concentration of the reactants and the total site density

[35]. Here, the equilibrium constant for the pseudo-second order kinetic model was 0.02 g/mg.h (Table 1) and a high initial AMI concentration (500 mg/L) was used throughout the adsorption kinetic experiment which partially corroborated with the hypothesis postulated by Reggazoni [34]. Cation exchange was identified as the mechanisms of AMI adsorption onto the SWy-2 clay mineral (Fig. 2a), which was also supported by the pseudo-second order kinetic model [15]. The kinetic study also showed that adsorption of AMI was relatively fast and reached 84% of the maximum adsorption capacity within 1 h, indicating a much faster adsorption of AMI onto the SWy-2 clay mineral adsorbent than other adsorbents such as palygorskite and kaolinite where intercalation of AMI was not likely to occur easily [16, 35].

3.2 Adsorption isotherm

AMI adsorption isotherm data were fitted to the Langmuir and Freundlich isotherm models (Supplementary Material; Fig. S3a-b), and results suggested that the experimental data were best fitted to the Langmuir model (R^2 = 0.66; RPD = 2.06) (Table 2). The maximum adsorption capacity for AMI was 276.3 mg/g (Table 2), which was well above 120, 76, 53 and 4.7 mg/g previously observed for activated carbon, granular activated carbon, palygorskite and kaolinite, respectively [16, 35-37], but was slightly below the value of 330 mg/g previously observed for Ca-montmorillonite [15]. This indicated that not only was the type of adsorbent important, but

263 for the same clay mineral the main counter ion was also important in determining AMI's
264 maximum adsorption capacity. Furthermore, the good fit to the Langmuir adsorption isotherm
265 suggested that monolayer adsorption of AMI occurred on the clay mineral surface of SWy-2,
266 since this one of the underlying assumptions of the Langmuir adsorption isotherm.
267 Regeneration of SWy-2 was conducted by a heat treatment (600ºC, 2 h) of the AMI-loaded
268 sample to enhance potential reuse during environmental remediation. Unlike the original SWy-2,
269 the isothermal AMI adsorption on the regenerated sample fit slightly better to the Freundlich
270 model rather than Langmuir model (Table 2; Fig. S3c-d), which was most likely due to partial
271 change of the heterogeneous surfaces on the clay mineral following the heat treatment. After one
272 cycle of regeneration, the material displayed a reasonable 71.7 mg/g adsorption capacity (~26%
273 of the original adsorbent) (Table 2), indicating potential for reuse in AMI removal from
274 wastewater.
275
276 *3.3 Desorbed cations*
277 The concentration of desorbed cations from SWy-2 during AMI adsorption was positively
278 correlated ($R^2 = 0.984$) with the amount of AMI adsorbed (Fig. 2a). Specifically, the amounts of
279 K^+ released during exposure to AMI were lower than Na^+, and invariant with the amount of AMI
280 adsorbed. The amount of Mg^{2+} released was only slightly correlated with the amount of AMI

adsorbed, which was likely due to the higher MgO content of the SWy-2 clay mineral (Table S1). However, Na^+ seemed to be completely desorbed by deionized water even without any AMI adsorption after 24 h, and desorbed Na^+ even increased above the initial AMI concentration of 300 mg/L (Fig. 2b). While complete desorption of Na^+ derived from raw SWy-2 required 24 h to reach equilibrium (Fig. 2b), adsorption of AMI on SWy-2 needed only 4 h (Fig. 1a). Therefore, the release of Na^+ was not entirely caused solely by solvation in deionized water during AMI adsorption. Instead, some of the desorbed Na^+ ions were desorbed via AMI adsorption, and consequently cation exchange controlled the adsorption procedure even under low adsorbate concentrations.

The ratio of the total desorbed cations to adsorbed amounts of AMI was 1.02, which was obtained from the slope of a plot of the amount of AMI adsorbed versus the amount of cations desorbed (Fig. 2a), and indicated that cation exchange was the dominant mechanism for AMI adsorption on SWy-2 [15, 16]. The maximum AMI adsorption capacity of 276.3 mg/g, equivalent to 0.88 meq/g, was just slightly higher than the CEC of SWy-2 (0.85 meq/kg), and since AMI adsorption was also accompanied by cation desorption (Fig. 2), this suggested that CEC of SWy-2 was the main controlling factor for AMI adsorption rather than simple electrostatic attraction. Unlike raw SWy-2, after adsorption of AMI on to the regenerated SWy-2, the concentrations of Na^+, K^+, Mg^{2+} and Ca^{2+} in the supernatant was < 3 mg/L, which indicated that the adsorption

299 mechanism of AMI on the regenerated sample did not involve substantial cation exchange. This
300 is interesting, since it points to heat treatment regeneration fundamentally changing the removal
301 mechanism for AMI. However, a thorough analysis of the physiochemical properties of the
302 regenerated SWy-2 would be required to fully understand altered AMI adsorption mechanism,
303 which was not the focus of this study.
304
305 *3.4 Effect of system pH on AMI adsorption*
306 The solution pH oftenregulates contaminant adsorption through electrostatic attraction; which is
307 a function of the surface charge of the clay-mineral adsorbent [37-41]. Hence, potential variation
308 of adsoption capacity with pH becomes an important consideration. However, here the variation
309 in AMI adsorption capacities with pH was negligible (Fig. S4) despite the pH_{pzc} (the pH where
310 the net surface charge on the clay mineral surface is zero) of SWy-2 being 8.35 [25]. This
311 indicated that the pH_{pzc} was not the key factor determining AMI adsorption. For example, at an
312 initial AMI concentration of 500 mg/L, when the solution pH was > 9.4, the adsorption capacity
313 for AMI was still maintained at a relatively high value (199 mg/g), despite AMI being neutral
314 above pH 9.4 (Fig. S1b), and theoretically unable to participate in cation exchange. This suggests
315 that there must be some contribution to adsorption from specific chemical bonding between the
316 clay surface and the amine groups of AMI even in its neutral form. Thus, overall, the two key

317 factors governing AMI adsorption on SWy-2 seem to be a combination of CEC and high affinity
318 between SWy-2 and AMI in the aqueous system.
319
320 *3.5 Effect of temperature on SWy-2 adsorption*
321 The adsorption of AMI increased with an increase in temperature (Fig. S5), indicating an
322 endothermic adsorption process, when the initial AMI concentration was 500 mg/L and the
323 solution pH ranged between 7 and 8. Thermodynamic analysis under these conditions showed
324 that Gibbs free energy (ΔG) was negative (Table 3) and thus confirmed that adsorption was a
325 spontaneous process with high affinity between SWy-2 and AMI [42, 43]. This had initially been
326 demonstrated by the experimental isotherm and kinetic adsorption data but was quantified here
327 via thermodynamic analysis. Likewise, the positive value for ΔH confirmed that the adsorption
328 process was endothermic, and corroborated two previous studies that had shown endothermic
329 adsorption of AMI on Ca-montmorillonite and palygorskite [15, 16]. The relatively positive
330 value of ΔS, a measure of increased molecular morphology disorder, suggested that the reaction
331 was spontaneous due in part to an increase in system randomness as AMI molecules randomly
332 distributed across SWy-2 surfaces. The values of ΔG calculated in this study (–6.0 to –22
333 KJ/mol) were consistently less than the free energy of micellization [44]. This indicated that AMI
334 micelle formation on the surface of SWy-2 was not likely. Thus, for AMI adsorption on the

surface of SWy-2, physical adsorption, like cation exchange, took place rather than micellization [15, 16].

3.6 XRD analysis

While the normal d-value of SWy-2 with one hydrated layer is 12.5 Å [45], here raw SWy-2 had a d-value of 15.0 Å (Fig. 3a), which compared well with 15.1 Å for a previous study [46], and thus indicated that the clay used here contained two hydrated layers, potentially due to high humidity. Following exposure to increasing amounts of AMI, the d-value expanded to 16.9 Å, which was less than 18.7 Å observed for methylene blue adsorption on SWy-2 [46], and much less than 20.6 Å previously observed for AMI adsorption on SAz-2 [15]. The specific change in d-value depends on a variety of parameters including molecular size, contact model and adsorption capacity, which makes direct comparisons with disparate studies difficult. However, what is important to note is that the expandable amplitude of d-value across all studies plays a significant role in determining the morphology inside the interlayers of swelling clays such as SWy-2, SAz-1 and rectorite. Essentially the maximum interlayer d-value limits the space available to adsorb large molecules. However, the d-value is not always stable and as observed here, after heating at 600 °C for 3 h (Fig. 3b), the breakdown of the structure of SWy-2 resulted in disappearance of d_{001} reflection after adsorption. In addition, the inset SEM images (Fig. 3a-b)

showed different clay morphologies, being lamellar and highly textured, and massively granular, respectively, before and after heat treatment. After heating, the lumpy structure indicated partial decomposition of SWy-2 (Fig. 3b). However, despite this, after heating, the AMI adsorption capacity still reached 71.7 mg/g, indicating that despite partial decomposition SWy-2 could still be reasonably reused as a material for the treatment of wastewater containing antidepressants, albeit at a reduced capacity.

3.7 Derivative thermogravimetric (DTG) analyses

For SWy-2, the thermogravimetric (TG) and derivative of TG (DTG) exhibited a peak at 78 °C with a mass loss of 8.3%, corresponding to the removal of adsorbed water, and a subsequent peak at 115 °C attributed to interlayer water loss [47] (Fig. 4a). The total mass loss of adsorbed and interlayer waters was about 10% for SWy-2, which gradually decreased to 5 and 2% as CEC increased from 0.71 to 1.03 (Fig. 4a). This indicated that AMI replaced water in the interlayers. The increase in total mass loss suggested the presence of AMI either on the surface or in the interlayer of SWy-2 (Fig. 4a). In comparison, AMI by itself exhibited a 99.5% mass loss (Fig. 4a), with a decomposition temperature of 270°C. The increase in AMI decomposition temperature to 281°C after adsorption (Fig. 4b) was attributed to AMI-clay intercalation [15, 48]. The total mass loss of 1.03 CEC was about 17% at 600°C (Fig. 4a), which was slightly lower

than the amount of AMI adsorbed on to SWy-2 (276 mg/g) corresponding to a total mass loss of 22%. Thus, the mass loss of SWy-2 loaded with AMI at the highest level of 1.03 CEC agreed well with the data obtained from the isotherm study.

3.8 FTIR analysis

The FTIR spectra (Fig. 5) showed characteristic bands attributable to AMI at 1252, 1163 and 1097 cm^{-1} suggesting the presence of C-N stretching vibrations of the $(CH_3)_2$-N-CH_2- groups [49]. However, Si–O vibrations were also observed in the range of 600–1600 cm^{-1} [50], masking some expected AMI bands (Fig. 5). Bands at 3057 and 3011 cm^{-1} corresponding to aromatic =C-H stretching vibrations in AMI shifted to 3047 and 3006 cm^{-1}, respectively, in 1.03 CEC SWy-2-AMI (Fig. 5). A broad band (Fig. 5) in the region 2400–2700 cm^{-1} was attributed to amine N-H groups [51], and was shifted considerably towards higher frequencies. Overall, the FTIR results showed the involvement of N-atoms (from the amine group) of the aliphatic chain of AMI during AMI adsorption in the SWy-2 interlayer, which indicated some degree of chemisorption reaction [52]. The strongest band at 750 cm^{-1} corresponded to hydrogens on the benzene ring of AMI molecule [53], being shifted to 775 cm^{-1} after intercalating into the interlayer of SWy-2. The intensity of the above peak increased as the amount of AMI adsorption increased (Fig. 5), confirming the preservation of AMI after

389 intercalation [52].

390

391 *3.9 Adsorption mechanism and interlayer morphologies*

392 The maximum AMI adsorption capacity of SWy-2 was slightly higher than the CEC of the clay

393 mineral (1.03 CEC equivalents). The slope of a plot of total ions desorbed versus the amount of

394 AMI adsorbed was 1.02 (Fig. 2a), which suggested a cation exchange mechanism was involved.

395 In addition, since variation in solution pH did not significantly influence the amount of AMI

396 adsorbed (Fig. S4), this suggested high affinity between AMI and SWy-2 independent of either

397 clay surface or AMI charge.

398 Since the size of the T-O-T layer in a 2:1 structure clay mineral is about 6.6 Å [54], compared to

399 a d-value for the 1.03 CEC clay sample of 16.9 Å (Fig. 3), the interlamellar space of SWy-2 had

400 about 10.3 Å left for accommodating AMI molecules which had dimensions of 10.68 Å×8.57

401 Å×5.89 Å. The calculated occupied areas of AMI molecules were 60.0, 30.0, 15.0, 10.0, 7.6, 6.2,

402 5.2, 4.7 and 4.3 $Å^2$ corresponding to 0.7, 0.15, 0.30, 0.44, 0.58, 0.71, 0.84, 0.94 and 1.02 CEC

403 equivalent adsorption capacity of the clay mineral, respectively. Since the occupied area of an

404 AMI molecule laying on the surface of SWy-2 in a horizontal alignment (91.5 $Å^2$) was greater

405 than the maximum calculated area (60 $Å^2$), this indicated that AMI could not wholly habitat the

406 clay horizontally. However, the AMI molecule could be still vertically aligned either within the

407 interlayer or on the surface. However, this also seemed unlikely because and occupied area
408 would still be 50.5 $Å^2$ which was still unsuitable for a vertical aligned inclusion of AMI. From
409 the 3D view, the length and width of AMI were 9.5 Å and 8.3 Å, respectively. Examination of
410 side view of the 3D clay and molecular models indicated that it was theoretically possible for
411 AMI to be adsorbed on the interlayer corresponding to the minima calculated occupied area with
412 contact between NH_2 groups attached to SWy-2 surfaces (Fig. 6a), as was indicated by the FTIR
413 results (Fig. 5). Consequently, the most reasonable contact model was obtained for 1.03 CEC
414 (Fig. 6a) which showed AMI tilted in the interlayer.
415 While the ideal contact model of AMI was initially proposed based on FTIR results (Fig. 6a), the
416 actual morphologies could be different from a 3D perspective. Therefore, molecular simulations,
417 were conducted using either two, three or four AMI molecules within 12 unit cells, which
418 reasonably mimicked practical changes from low to high adsorbed capacities. This simulation
419 showed the same contact model, which was interacted through the NH_2 group and benzene ring
420 of AMI (Fig. 6 b-d), and close interaction of the four vertically orientated AMI molecules as one
421 layer within the basal planes of SWy-2 (Fig. 6d). These theoretical calculations thus supported
422 the observed experimental results, and suggested that for AMI, the swelling of the interlayer
423 space of SWy-2 limited the options for AMI interlayer morphology to one layer even though the
424 maximum adsorbed capacity suggested AMI could potentially occupy two layers [15].

4. Conclusions

This study for the first time reports on the adsorptive removal of an antidepressant drug AMI from water using a naturally available Na-montmorillonite (SWy-2), describing the drug adsorption behavior, mechanisms and reusability of the adsorbent. Montmorillonite was shown to have significant advantages as an antidepressant drug absorbent being inexpensive, with high cation exchange capacity, which make this material appropriate for the treatment of both industrial and domestic wastewater loaded with cationic drug compounds. The removal of AMI by SWy-2 was relatively fast (< 4 h), and efficiently, with an optimal adsorption capacity of 276 mg/g corresponding to 0.88 meq/g, which was slightly higher than the total CEC of 0.86 meq/g of SWy-2. AMI adsorption was best described by the Langmuir isotherm model. Adsorption of AMI coincided with desorption of inorganic cations, which indicated that the main mechanism of AMI removal was via cation exchange of AMI^+ by mainly Na^+ in SWy-2. AMI adsorption on SWy-2 was independent of the solution pH. Thermodynamic analysis revealed that AMI adsorption on SWy-2 was endothermic, where AMI adsorption increased with temperature. The small positive value of ΔS suggested that the adsorbed AMI molecules adopted a random arrangement on the SWy-2 surfaces or in the interlayers. The participation of the amine and benzene groups of AMI in a tilted one layer orientation in the interlayers of SWy-2 was indicated

by molecular simulations, and was confirmed by XRD, TGA and FTIR results. Future research needs to be conducted to verify the performance of SWy-2 clay mineral in removing antidepressant drugs from real wastewater, and optimizing the process parameters in pilot scale application under column filtration system, as well as more practically efficient methods for the regeneration of the spent adsorbent.

Acknowledgements

This research gratefully acknowledges the financial support via grant SJ201910698350 and 1191319102 from Xi'an Jiaotong University, Shaanxi, P.R. China. The authors are thankful to the core facilities sharing platform instrumental access including HPIC, XRD, FE-SEM, TGA, FTIR for the analyses of samples at Xi'an Jiaotong University, and the students of Chen Tan, Xiao-Yan Sun and Yu Tian. The authors are also thankful to Prof Tao Yang at Xi'an Jiaotong University for support and suggestions in the molecular simulation exercise. Binoy Sarkar acknowledges the support from Lancaster Environment Centre Project.

Credit author statement

Po-Hsiang Chang: Conceptualization and experimental design, Fund acquisition, supervision and preparation of first draft of the manuscript, Data checking, analysis, modelling, and revision.

Result interpretation and improvement of the manuscript. Pan Liu: Experiments and instrumental analysis. Binoy Sarkar: Conceptualization and experimental design, Data checking, analysis, modelling, and revision, Result interpretation and improvement of the manuscript. Raj Mukhopadhyay: Data checking, analysis, modelling, and revision, Result interpretation and improvement of the manuscript. Qing-Yuan Yang: Conceptualization and experimental design, Fund acquisition. Yu-Min Tzou: Result interpretation and improvement of the manuscript. Bo Zhong: Result interpretation and improvement of the manuscript. Xuxiang Li: Result interpretation and improvement of the manuscript. Gary Owens: Data checking, analysis, modelling, and revision, Result interpretation and improvement of the manuscript.

References

[1] B. Ren, X. Shi, X. Jin, X.C. Wang, P. Jin, Chem. Eng. J. 404 (2021) 127024.

[2] L. Gunnarsson, J.R. Snape, B. Verbruggen, S.F. Owen, E. Kristiansson, L. Margiotta-Casaluci, T. Österlund, K. Hutchinson, D. Leverett, B. Marks, C.R. Tyler, Environ. Int. 129 (2019) 320.

[3] L.A. Thompson, W.S. Darwish, J. Toxicol. (2019) 2345283.

[4] Y. He, D.B. Jiang, J. Chen, D.Y. Jiang, Y.X. Zhang, J. Colloid Interface Sci. 510 (2018) 207.

[5] B. Sarkar, R. Rusmin, U.C. Ugochukwu, R. Mukhopadhyay, K.M. Manjaiah, Chapter 5 -

Modified clay minerals for environmental applications. In: Mercurio, M., Sarkar, B., Langella, A., eds. Modified Clay and Zeolite Nanocomposite Materials. Elsevier, 2019. p. 113.

[6] P. Bottoni, S. Caroli, A.B. Caracciolo, Environ. Toxicol. Chem. 92 (2010) 549.

[7] M. Carballa, F. Omil, J.M. Lema, M. Llompart, C. Garcia-Jares, I. Rodriguez, M. Gome, T. Ternes, Water Res. 38 (2004) 2918.

[8] S.K. Khetan, T.J. Collins, Chemical Rev. 107 (2007) 2319.

[9] OECD Environment Directorate, Pharmaceutical residues in freshwater: hazards and policy responses, OECD Policy Highlights 2019.

[10] M. Bilal, M. Adeel, T. Rasheed, Y. Zhao, H.M.N. Iqbal, Environ Int. 124 (2019) 336.

[11] S. Doyle, E. Meade, C. Fowley, M. Garvey, Eur. J. Exp. Biol. 10 (2020) 2:5.

[12] N. Nijsingh, C. Munthe, D.G. J. Larsson, Environ. Health 18 (2019) 1.

[13] M. Klavairoti, D. Mantzavinos, D. Kassinos, Environ. Int. 35 (2009) 402.

[14] S.A. Kraemer, A. Ramachandran, G.G. Perron, Microorganisms 7 (2019) 1.

[15] P.-H. Chang, W.-T. Jiang, Z. Li, C.-Y. Kuo, J.-S. Jean, W. –R. Chen, G. Lv, J. Hazard. Mater. 277 (2014) 44.

[16] Y.-L. Tsai, P.-H. Chang, Z.-Y. Gao, X.-Y. Xu, Y.-S. Chen, Z.-H. Wang, X.-Y. Chan, Z.-Y. Yang, Z.-H. Wang, J.-S. Jean, Z. Li, W.-T. Jiang, Chemosphere 155 (2016) 292.

[17] E.J. Franssen, P.W. Kulast, P.M. Bet, R.J.M. Strack van Schijndel, A.C. van Loenen, A.J. Wilhelm, Ther. Drug Monit. 25 (2003) 248.

[18] M.M. Khalid, M.D. Cruz, D. Vearrier, M. I. Greenberg, Clin. Toxicol. 57 (2019) 825.

[19] H.K. Thanacoody, S.H. Thomas, Toxicol. Rev. 24 (2005) 205.

[20] N.A. Buekley, I.M. Whyte, A.H. Dawson, P.R. McManus, N.W. Ferguson, Med. J. Aust. 162 (1995) 190.

[21] S.H.L. Thomas, L. Bevan, S. Bhattacharyya, Hum. Exp. Toxicol. 15 (1996) 466.

[22] A.L. Green, J. Pharm. 19 (1967) 10.

[23] S. Bindya, W.-T. Wong, M.A. Ashok, H.S. Yathirajan, R.S. Rathore, Acta Crystallogr. C Struct. Chem. 63 (2007) 546.

[24] R. Mukhopadhyay, T. Adhikari, B. Sarkar, A. Barman, R. Paul, A. K. Patra, P. C. Sharma, P. Kumar, J. Hazard. Mater. 376 (2019) 141.

[25] P. Stathi, K. Litina, D. Gournis, T.S. Giannopoulos, Y. Deligiannakis, J. Colloid Interface Sci. 316 (2007) 298.

[26] H. Van Olphen, J.J. Fripiat, Data Handbook for Clay Materials and Other Non-metallic Minerals. Pergamon Press, New York (1979).

[27] Q.H. Zeng, A.B. Yu, G.Q. Lu, R.K. Standish, Chem. Mater. 15 (2003) 4732.

[28] G. Lv, L. Liu, Z. Li, L. Li, M. Liu, J. Colloid Interface Sci. 374 (2012) 218.

[29] Y.S. Ho, G. McKay, Process Biochem. 34 (1999) 451.

[30] J.M. Jabar, Y.A. Odusote, K.A. Alabi, I.B. Ahmed, Appl. Water Sci. 10 (2020) 136.

[31] J. Bujdák, Appl. Clay Sci. 191 (2020) 105630.

[32] S. Dacrory, El S.A. Haggag, A.M. Masoud, S.M. Abdo, A.A. Eliwa, S. Kamel, Cellulose 27 (2020) 7093.

[33] Y. Park, G.A. Ayoko, E. Horváth, R. Kurdi, J. Kristof, R.L. Frost, J. Colloid Interface Sci. 393 (2013) 319.

[34] A.E. Regazzoni, Colloid Surface A. 585 (2020) 124093.

[35] G. Lv, C. Stockwell, J. Niles, S. Minegar, Z. Li, W.-T. Jiang, J. Colloid Interface Sci. 411 (2013) 198.

[36] J.M.V. Nabais, B. Ledesma, C. Laginhas, Adsorp. Sci. Technol. 30 (2012) 255.

[37] B. Ledesma, S. Roman, J.F. Gonzalez, F. Zamora, M.C. Rayo, Adsorp. Sci. Technol. 28 (2010) 739.

[38] M. H. Derkani, A. J. Fletcher, M. Fedorov, W. Abdallah, B. Sauerer, J. Anderson, Z.J. Zhang, Colloids Interfaces 3 (2019) 62.

[39] L. Hou, Q. Liang, F. Wang, RSC Adv. 10 (2020) 2378.

[40] D. Vasudevan, G.L. Bruland, B.S. Torrance, V.G. Upchurch, A.A. MacKay, Geoderma 151 (2009) 68.

[41] Y. Xu, X. Yu, B. Xu, D. Peng, X. Guo, Sci. Total Environ. 753 (2021) 141891.

[42] H.H. Eldaroti, S.A. Gadir, M.S. Refat, A.M.A. Adam, J. Pharmaceut. Anal. 4 (2014) 81.

[43] Y. El Maguana, N. Elhadiri, M. Benchanaa, R. Chikri, J. Chem. (2020) 9165874.

[44] Kabir-ud-Din, M.A. Rub, A.Z. Naqvi, Colloid Surface B 82 (2011) 87.

[45] J.M. Cases, I. Bérend, G. Besson, M. Francois, J.P. Uriot, Q.F. Thomas, J.E. Poirier, Langmuir 8 (1992) 2730.

[46] Z. Li, P.-H. Chang, W.-T. Jiang, J.-S. Jean, H. Hong, Chem. Eng. J. 168 (2011) 1193.

[47] S. Guggenheim, A.F.K. Groos, Clay Clay Miner. 49 (2001) 433.

[48] Z. Li, W.-T. Jiang, Thermochimic. Acta. 483 (2009) 58.

[49] G. Socrates, Infrared Characterstic Group Frequencies, John Wiley & Sons, New York, 1980. p. 54.

[50] J. Madejová, P. Komadel, Clay Clay Miner. 49 (2001) 410.

[51] N. Rahman, S. Khan, J. Electroanal. Chem. 777 (2016) 92.

[52] W. Misiuk, H. Puzanowska-Tarasiewiez, Anal. Lett. 35 (2002) 1163.

[53] K.W. Blessel, B.C. Rudy, B.Z. Senkowski, Anal. Profiles Drug Subst. 3 (1974) 127.

[54] C. Robert, J.R. Reynolds, X-ray diffraction and the identification and analysis of clay minerals, Oxford New York, 1989. P. 332.

551 **Table captions**

552 **Table 1**. Estimated best fit kinetic model parameters for AMI adsorption on SWy-2.

553 **Table 2.** Estimated best fit isothermal model parameters for AMI adsorption on the original and

554 regenerated SWy-2 (600ºC, 2 h).

555 **Table 3.** Thermodynamic parameters for AMI adsorption on SWy-2 under different

556 temperatures.

557

558 **Figure captions**

559 **Fig. 1.** Adsorption of AMI on SWy-2; (a) adsorption kinetics (pH 7, AMI concentration 500

560 mg/L) (with best fitted pseudo-second order kinetic plot), (b) adsorption isotherm (with best

561 fitted Langmuir isotherm plot) for the original SWy-2 (at pH 7~8), and (c) adsorption isotherm

562 (with best fitted Freundlich isotherm plot) for the regenerated SWy-2 (heated at 600ºC, at pH

563 7~8). Data points represent average of duplicated results.

564 **Fig. 2.** Desorption of metal cations from SWy-2 (a) as affected by the amounts of AMI adsorbed,

565 and (b) as affected by equilibrium time in deionized water. Data points represent average of

566 duplicated results.

567 **Fig. 3.** XRD patterns of original SWy-2 and SWy-2 with different amounts of AMI intercalated

568 having SEM image of 1.03 CEC sample in the inset (a), and the XRD patterns of regenerated

samples (600°C, 2 h) with SEM images of original SWy-2 (below) and the regenerated sample (top) in insets (b).

Fig. 4. TG analyses of SWy-2, and SWy-2 with AMI adsorbed amounts equivalent to 0.15, 0.71 and 1.03 CEC of the clay mineral (a), and corresponding DTG curves (b). The vertical scale of figures for raw AMI is on the right side, whereas those for AMI loaded on SWy-2 are on the left side.

Fig. 5. FTIR spectra of SWy-2, AMI, and AMI loaded on SWy-2 in amounts equivalent to 0.15 and 1.03 CEC of the clay mineral.

Fig. 6. Illustration of intercalated AMI in the interlayer of SWy-2 based on FTIR signals at high AMI loading (a), and molecular simulations under two, three and four molecules of AMI within 12 unit cells of the clay mineral (b, c, d).

Tables

Table 1. Estimated best fit kinetic model parameters for AMI adsorption on SWy-2.

Pseudo-first order		Pseudo-second order		Intra-particle diffusion		Elovich	
Parameter	Value	Parameter	Value	Parameter	Value	Parameter	Value
q_e (mg/g)	185.9	q_e (mg/g)	201.1	k_{id} (mg/g.$h^{1/2}$)	18.9	α (mg/g.h)	26.8
k_1 (/h)	1.97	k_2 (g/mg.h)	0.02	Θ (mg/g)	122.1	ß (g/mg)	0.05
R^2	0.98	R^2	0.98	R^2	0.52	R^2	0.76
Adj R^2	0.97	Adj R^2	0.98	R^2_{adj}	0.49	R^2_{adj}	0.75
RMSEP	6.34	RMSEP	5.48	RMSEP	27.96	RMSEP	19.80
RPD	6.30	RPD	6.97	RPD	1.02	RPD	1.73

R^2: co-efficient of determination; R^2_{adj}: adjusted co-efficient of determination; RMSEP: root mean square error of prediction; RPD: ratio of performance to the deviation.

586 **Table 2**. Estimated best fit isothermal model parameters for AMI adsorption on the original and

587 regenerated SWy-2 (600ºC, 2 h).

Parameter	Adsorbent	
	SWy-2	Regenerated SWy-2
Freundlich model		
K_F [(mg/g) (L/mg)$^{1/n}$]	87.0	40.9
1/n (L/g)	0.21	0.12
R^2	0.54	0.84
Adj R^2	0.51	0.83
RMSEP	61.40	8.23
RPD	1.52	3.01
Langmuir model		
q_m (mg/g)	276.3	71.7
b (L/mg)	0.14	7.62
R^2	0.66	0.64
Adj R^2	0.64	0.62

RMSEP	52.58	12.36
RPD	2.06	1.88

588

589 **Table 3.** Thermodynamic parameters of AMI adsorption on SWy-2 under different temperatures

pH	Ln K_c			△G (kJ/mol)			△H (kJ/mol)	△S (kJ/mol K)
	303K	318K	333K	303K	318K	333K		
7.0-8.0	3.31	4.38	8.66	-6.95	-14.63	-22.31	148.20	0.51

590

591

592 **Figures**

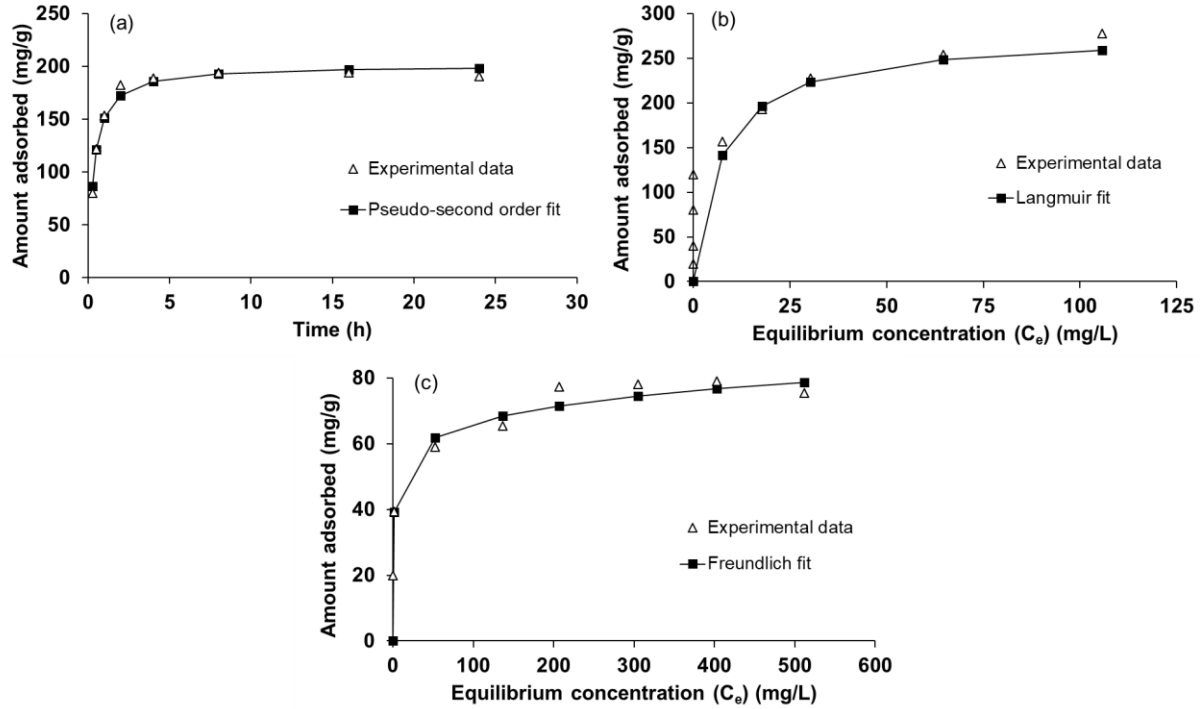

593

594 Fig. 1.

595

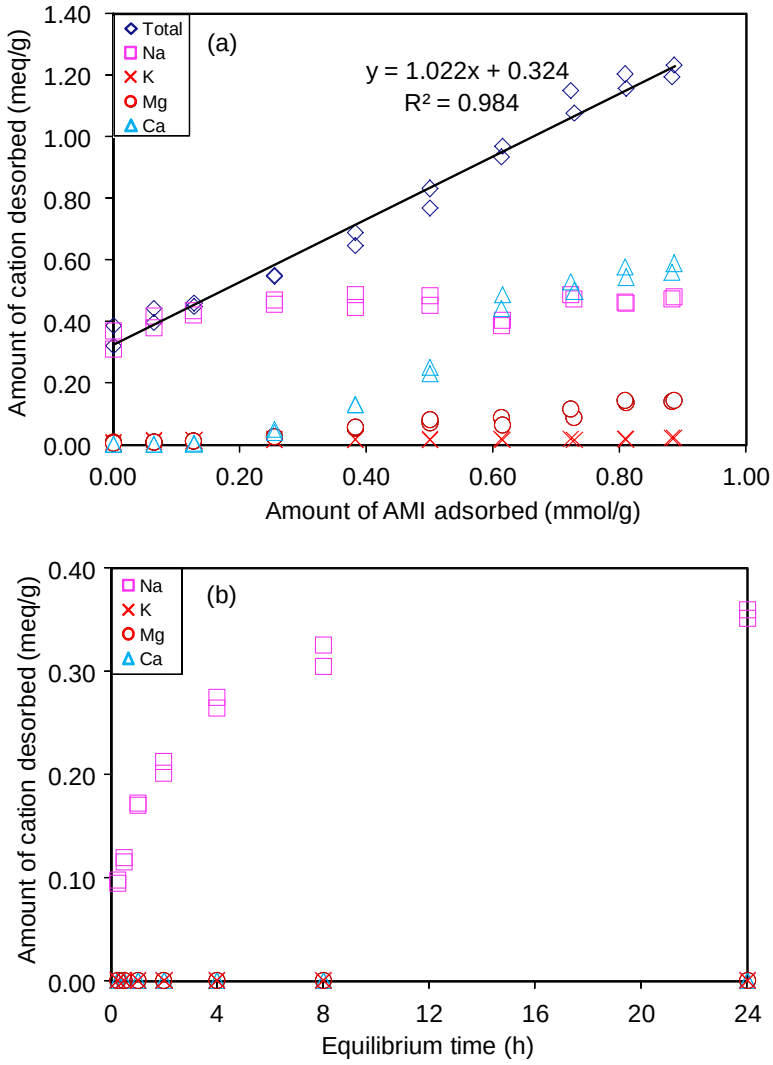

596

597 Fig. 2.

598

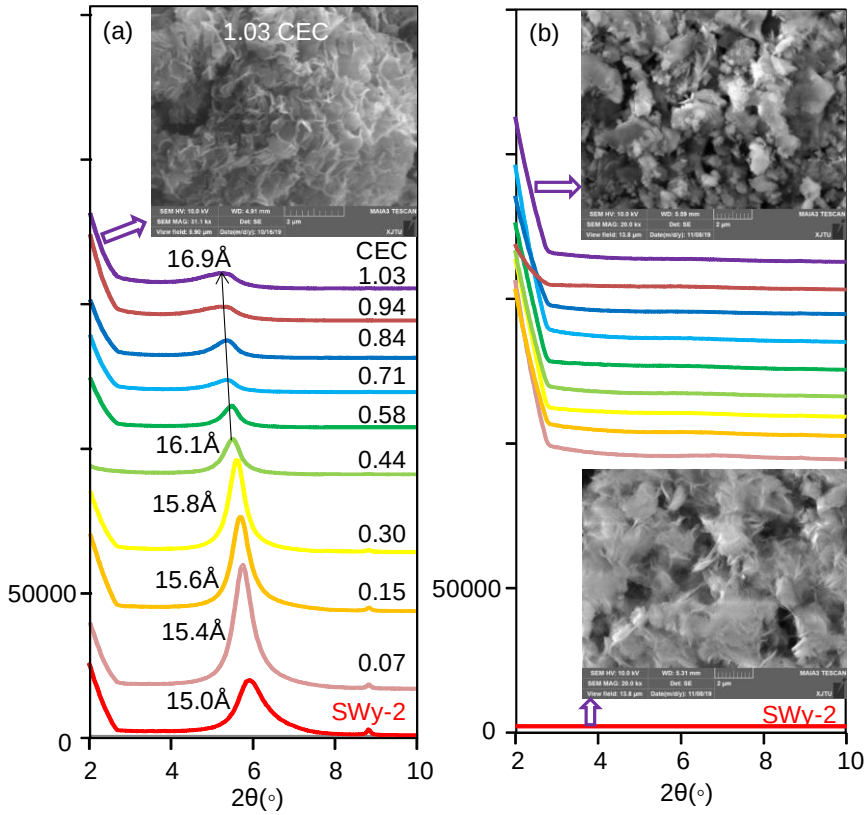

599

600 Fig. 3.

601

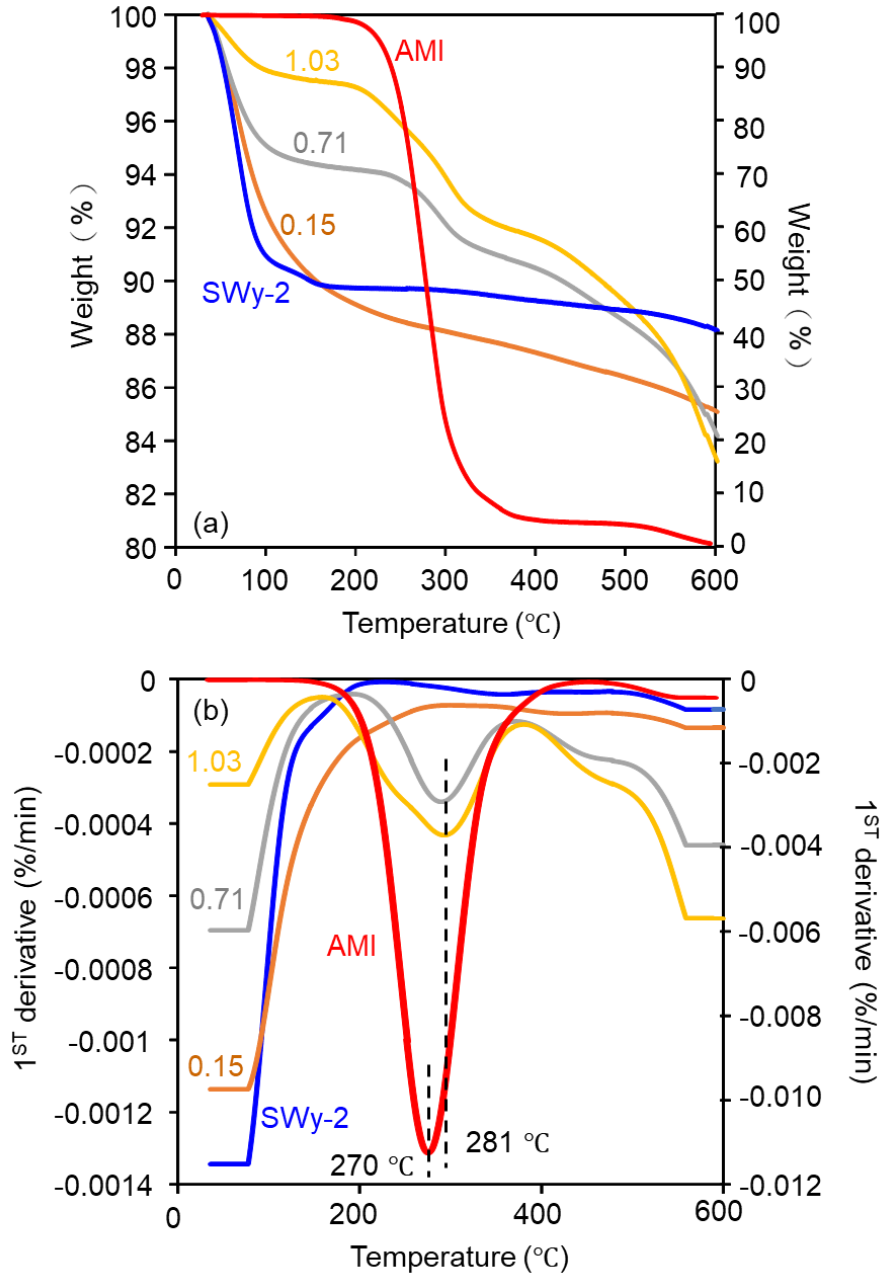

602

603 Fig. 4.

604

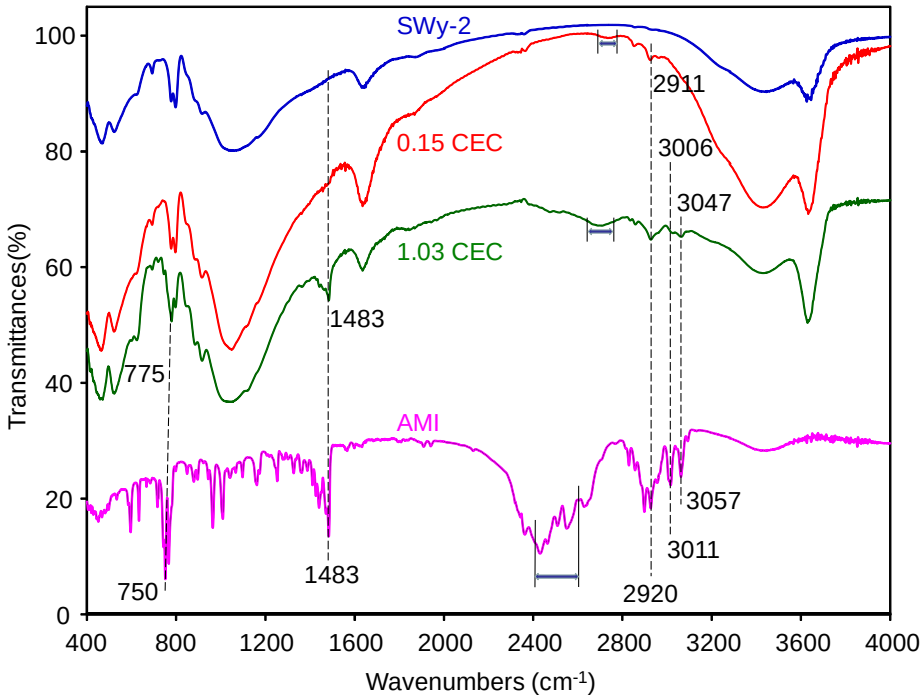

605

606 Fig. 5.

607

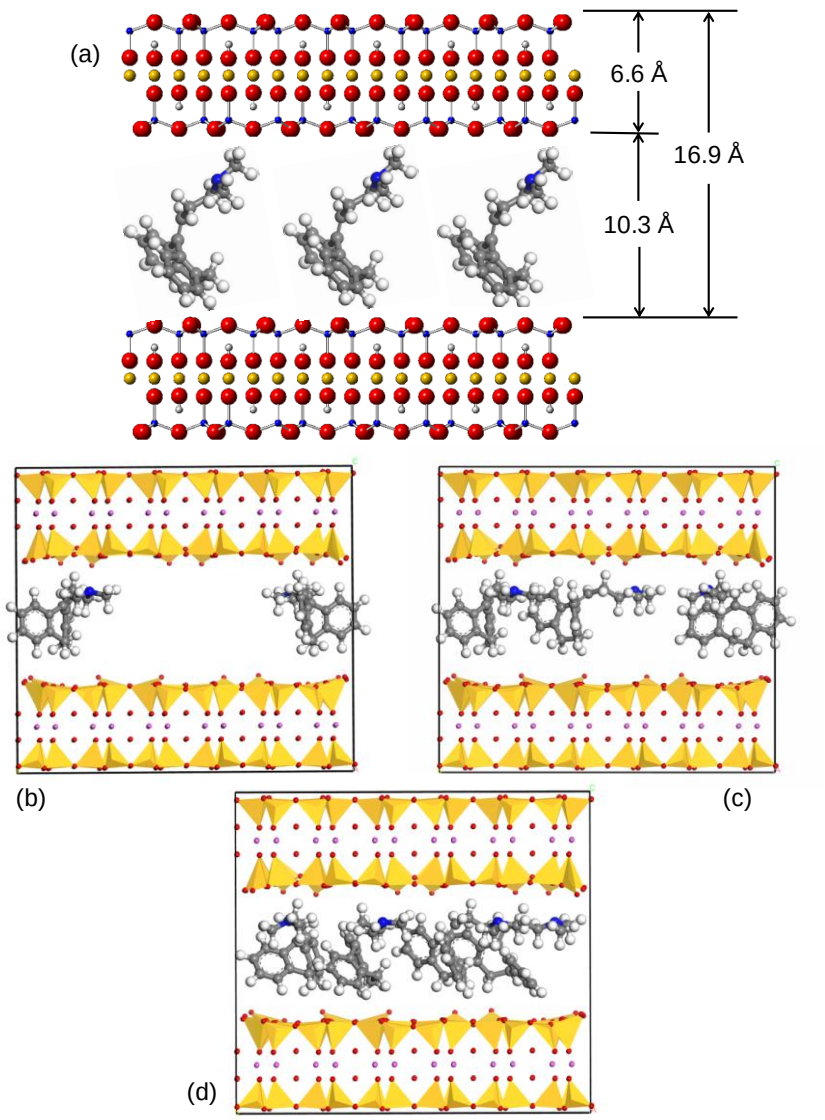

608

609 Fig. 6.

610

Supplementary Material for:

Unravelling the mechanism of amitriptyline removal from water by natural montmorillonite through batch adsorption, molecular simulation and adsorbent characterization studies

Po-Hsiang Chang[a], Pan Liu[a], Binoy Sarkar[b,*], Raj Mukhopadhyay[c], Qing-Yuan Yang[d,*], Yu-Min Tzou[e], Bo Zhong[a], Xuxiang Li[a], Gary Owens[f]

[a] School of Human Settlements and Civil Engineering, Xi'an Jiaotong University, 28 Xianning West Road, Xi'an, Shaanxi, 710049, P.R. China

[b] Lancaster Environment Centre, Lancaster University, Lancaster, L A1 4YQ, United Kingdom

[c] Division of Irrigation and Drainage Engineering, ICAR-Central Soil Salinity Research Institute, Karnal – 132001, Haryana, India

[d] School of Chemical Engineering and Technology, Xi'an Jiaotong University, 28 Xianning West Road, Xi'an, Shaanxi, 710049, P.R. China

[e] Department of Soil and Environmental Sciences, National Chung Hsing University, 145 Xingda Rd., Taichung, 40227, Taiwan

[f] Environmental Contaminants Group, Future Industries Institute, University of South Australia, Mawson Lakes, SA 5095, Australia

*Co-corresponding authors:

Dr Binoy Sarkar; Lancaster University; email: b.sarkar@lancaster.ac.uk

Prof Qing-Yuan Yang; Xi'an Jiaotong University; email: qingyuan.yang@xjtu.edu.cn

SI texts

1. Kinetic models

The AMI adsorption kinetic data were fitted to pseudo-first order, pseudo-second order, intra-particle diffusion, and Elovich models by non-linear regression using least square methods. The empirical equations are given below.

Pseudo-first order: $q_t = q_e (1- e^{-k_1 t})$ (Eq. 1)

Pseudo-second order: $q_t = q_e^2 k_2 t/ (1 + q_e k_2 t)$ (Eq. 2)

Intra-particle diffusion: $q_t = k_{id} t^{1/2} + \theta$ (Eq. 3)

Elovich: $q_t = 1/\beta \ln (\alpha\beta) + (1/\beta) \ln t$ (Eq. 4)

where, q_e is the equilibrium amount of adsorption of AMI on the SWy-2 adsorbent (mg/g), k_1 is the rate constant of pseudo first-order adsorption (/h); k_2 is the equilibrium rate constant of pseudo second-order (g/mg.h); k_{id} is the rate constant (mg/g.h$^{1/2}$), and θ (mg/g) is the intercept. α is the adsorption rate (mg/g.h), and β is the desorption constant (g/mg) during the experiment.

2. *Isothermal models*

The AMI adsorption isotherm data of the original SWy-2 and the regenerated adsorbent (heated at 600 ºC for 2 h) were fitted to Langmuir and Freundlich isotherm equations by non-linear regression using least square methods. The empirical equations are detailed below.

Langmuir isotherm: $q_e = (b\ C_e\ q_m)/(1 + b\ C_e)$ (Eq. 5)

Freundlich isotherm: $q_e = K_F\ C_e^{1/n}$ (Eq. 6)

where, C_e is the equilibrium concentration of AMI (mg/L), q_e is the amount of AMI adsorbed (mg/g), q_m is the potential adsorption maxima of AMI on SWy-2 (mg/g), b is the bonding energy constant or Langmuir constant (L/mg), and K_F [(mg/g) $(L/mg)^{1/n}$] and 1/n (L/g) are the Freundlich constant at equilibrium and exponential factor, respectively.

3. *Data modelling*

The details of formula for co-efficient of determination (R^2) (Eq. 7), adjusted co-efficient of determination (R^2_{adj}) (Eq. 8), root mean square error of prediction (RMSEP) (Eq. 9), and ratio of performance to the deviation (RPD) (Eq. 10) are given below:

$$R^2 = 1 - [(\sum_i^n (q_{e'meas} - q_{e'calc})^2) \div (\sum_i^n (q_{e'meas} - q_{e'meas\ mean})^2)] \quad \text{(Eq. 7)}$$

$$R^2_{adj} = 1 - (1 - R^2).\ \frac{(n-1)}{(n-p)} \quad \text{(Eq. 8)}$$

$$RMSEP = \sqrt{\frac{1}{n-1}} \sum_i^n (q_{e'meas} - q_{e'calc})^2 \quad \text{(Eq. 9)}$$

$$RPD = SD/RMSEP \quad \text{(Eq. 10)}$$

where, n = number of data points; p = number of parameters in model equation, 'meas' means measured, and 'calc' means calculated.

4. Thermodynamic parameters

The thermodynamic parameters of AMI adsorption were deduced from the variation in thermodynamic equilibrium constant (K_c) with temperature. The K_c (dimensionless) value was obtained as the ratio of the amount of AMI adsorbed at equilibrium (C_a) (mg/L) to the amount of AMI in the solution at equilibrium (C_e) (mg/L). The initial AMI concentration was 500 mg/L. The thermodynamic parameters were calculated using Eq. 11 to 14 (Sarkar et al., 2012; Bhattacharya et al., 2008):

$$Kc = \frac{Ca}{C_e} \quad \text{(Eq. 11)}$$

$$\Delta G = -RT\,lnK_c \quad \text{(Eq.12)}$$

$$Ln\ Kc = -\frac{\Delta H}{RT} + \frac{\Delta S}{R} \quad \text{(Eq. 13)}$$

$$\Delta G = \Delta H - T\Delta S \quad \text{(Eq. 14)}$$

where, T is the temperature (K), R is the universal gas constant (8.314 J/mol•K), ΔH is the enthalpy change (kJ/mol), and ΔS is the entropy change (kJ/mol•K).

SI Figures

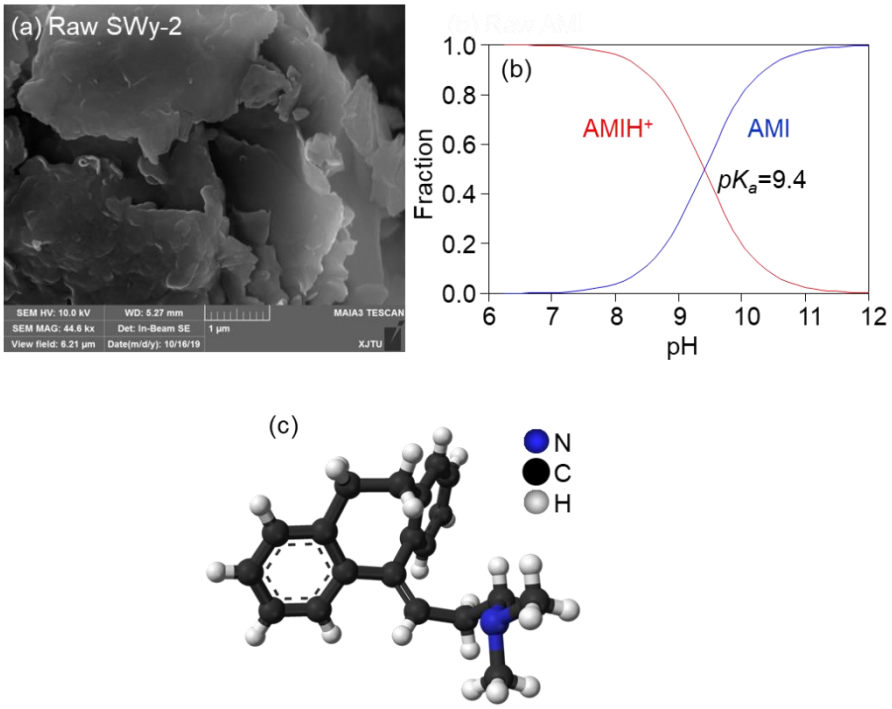

Fig. S1. SEM image of SWy-2 (a), speciation of AMI under different pH values (b), and the molecular structure of AMI (c).

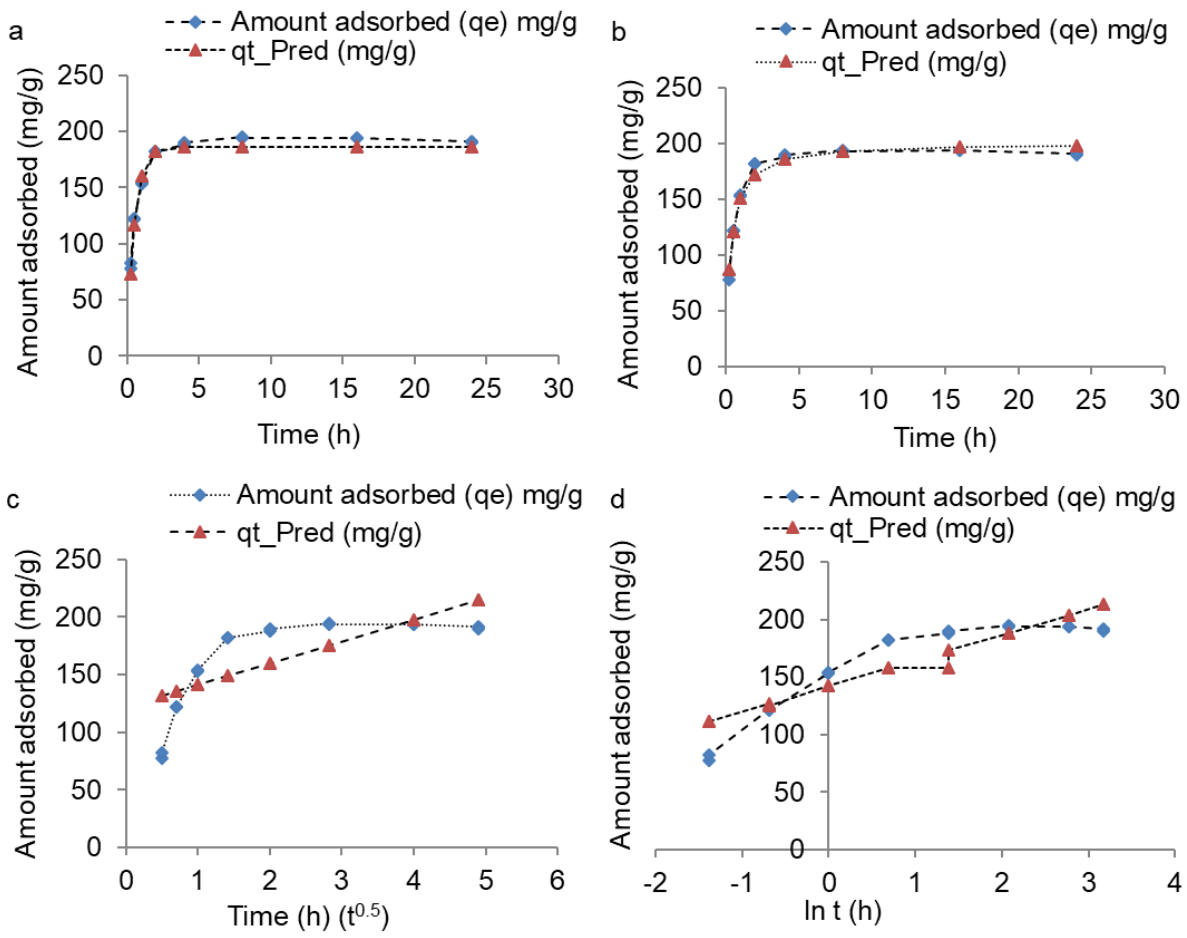

688

689 **Fig. S2.** Non-linear kinetic model fitting curves for AMI adsorption on SWy-2 (Experimental

690 conditions: pH = 7, initial AMI concentration = 500 mg/L); (a) pseudo-first order model, (b)

691 pseudo-second order model, (c) intra-particle diffusion model, and (d) Elovich model.

692

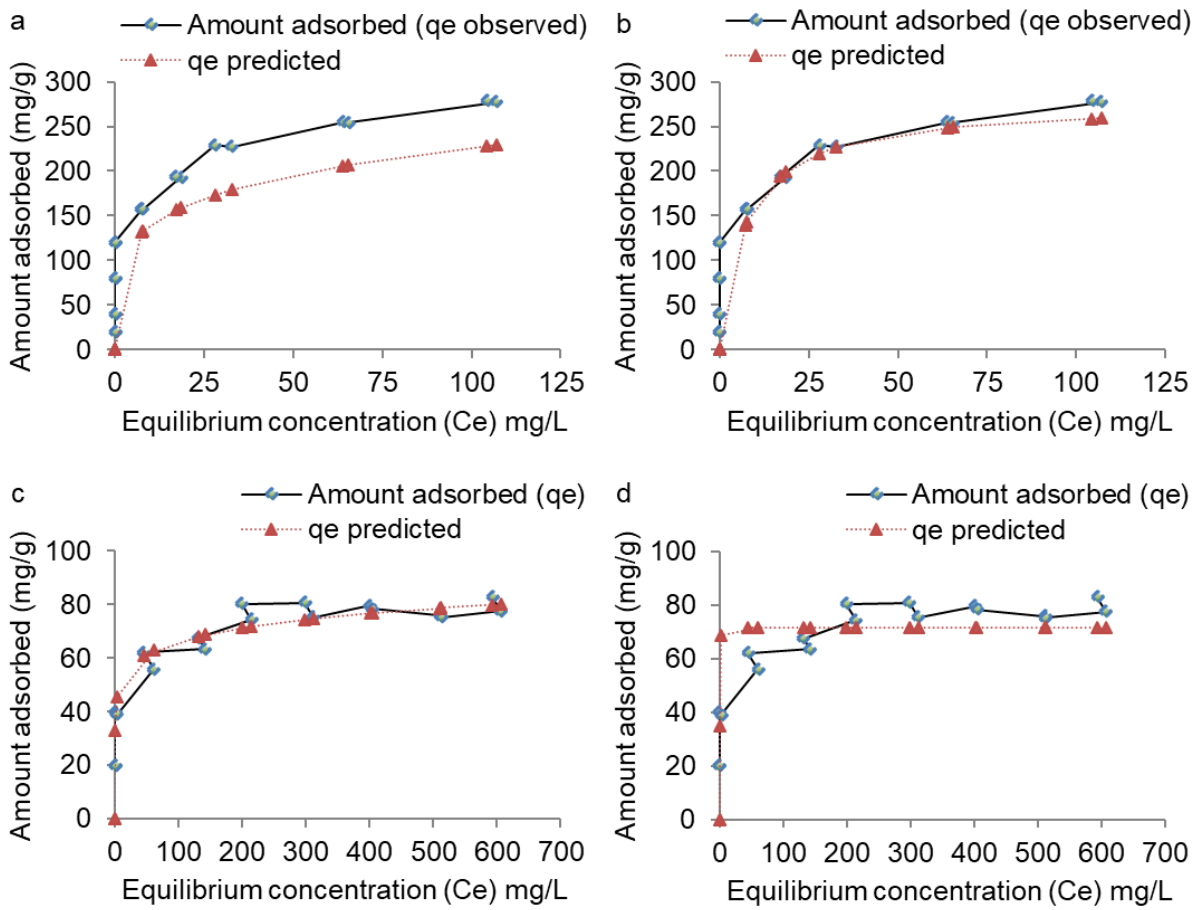

693

694 **Fig. S3.** Non-linear isotherm model fitting curves for AMI adsorption on original and regenerated

695 SWy-2 (600ºC, 2 h) (pH 7~8 for both experiments); (a-b) Freundlich and Langmuir models for

696 original SWy-2, and (c-d) Freundlich and Langmuir models for regenerated SWy-2.

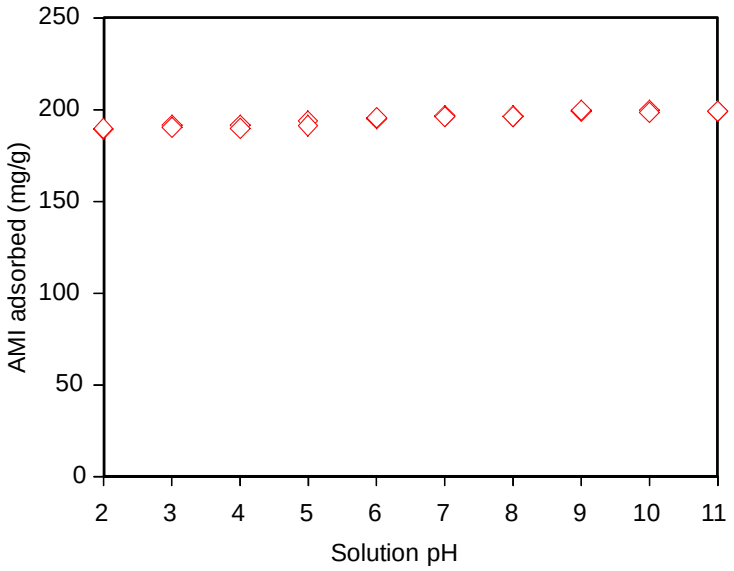

697

698

699 **Fig. S4.** AMI adsorption on SWy-2 as affected by equilibrium solution pH at an initial AMI

700 concentration of 500 mg/L.

701

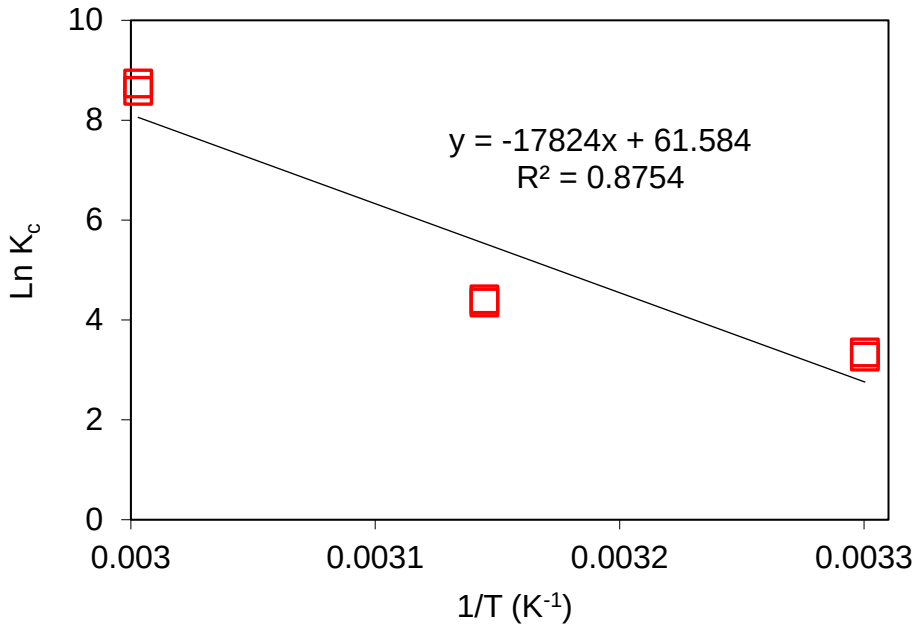

Fig. S5. AMI adsorption on SWy-2 as affected by equilibrium temperature at pH 7-8 at an initial AMI concentration of 500 mg/L.

706 **SI Tables**

707 **Table S1.** Physicochemical properties of SWy-2.

Physicochemical property	Values	References
Specific surface area	23 m^2/g	Dogan et al. (2006)
SiO_2	61.46%	Mermut and Cano (2001)
Al_2O_3	22.05%	Mermut and Cano (2001)
TiO_2	0.09%	Mermut and Cano (2001)
Fe_2O_3	4.37%	Mermut and Cano (2001)
MgO	2.94%	Mermut and Cano (2001)
CaO	1.18%	Mermut and Cano (2001)
Na_2O	1.47%	Mermut and Cano (2001)
K_2O	0.20%	Mermut and Cano (2001)
Cation exchange capacity (CEC)	0.85 meq/g	Borden and Giese (2001)
Point of zero charge (PZC)	8.35	Panagiota et al. (2007)

708

709

710 **References**

711 Bhattacharya, A., Naiya, T., Mandal, S., Das, S., (2008). Adsorption, kinetics and equilibrium

712 studies on removal of Cr(VI) from aqueous solutions using different low-cost adsorbents.
713 Chemical Engineering Journal 137 529-541.
714 Borden, D., Giese, R.F., (2001). Baseline studies of the clay minerals society source clays: Cation
715 exchange capacity measurements by the ammonia-electrode method. Clays and Clay
716 Minerals 49, 444–445.
717 Dogan, A.U., Dogan, M., Onal, M., Sarikaya, Y., Aburub, A., Wurster, D.E., (2006). Baseline
718 studies of the clay minerals society source clays: specific surface area by the brunauer emmett
719 teller (BET) method. Clays and Clay Minerals 54, 62–66.
720 Mermut, A., Cano, A.F., (2001). Baseline studies of the clay minerals society Source clays:
721 chemical analyses of major elements. Clays and Clay Minerals 49, 381–386.
722 Panagiota, S., Kiriaki, L., Dimitrios, G., Thomas, S.G., Yiannis, D., (2007). Physicochemical study
723 of novel organoclays as heavy metal ion adsorbents for environmental remediation. Journal
724 of Colloid and Interface Science 316, 298–309.
725 Sarkar, B., Megharaj, M., Xi, Y., Naidu, R., (2012). Surface charge characteristics of organo-
726 palygorskites and adsorption of *p*-nitrophenol in flow-through reactor system. Chemical
727 Engineering Journal 185–186, 35-43.
728